3B. Preparation of HPU/graphene oxide nanocomposite

3B.1. Introduction

Formation of the nanocomposite is a convenient approach to overcome the inadequacy of HPU as mentioned in sub-chapter 3A. In this context, much attention has been paid to PU nanocomposites with carbon based nanomaterials because the incorporation of carbon based nanomaterials can effectively enhance the thermal, mechanical and electrical properties of the pristine PU.[31] PU/CNT nanocomposites are frequently being reported in the literature.[32] However, the formation of macro/micro-aggregates in polymer matrices limits their uses in PU nanocomposites. To improve the dispersibility of CNT, surface modification is essential. Again, surface modification of CNT is difficult due to its inert nature.[33] In this regard, graphene oxide (GO) is an effective low-cost carbon based nanomaterial for obtaining desired PU nanocomposites as it is easy to prepare.[34,35] Also, GO possesses a substantial amount of oxygen-containing functional groups such as hydroxyl and epoxy on the basal planes and carboxyl and carbonyl groups on the edges of its.[9] This enables GO to be uniformly dispersed in the polymer matrices. Furthermore, GO exhibits analogous chemical properties to CNT and also possesses a similar structure to layered nanoclay.[36] Thus, it shows great potential in the development of nanocomposites with various desired properties such as mechanical, thermal, etc. Jing et al. prepared PU/GO nanocomposite by using the thermally induced phase separation (TIPS) technique.[37] The fabricated nanocomposite exhibited good mechanical and thermal properties. Ponnamma et al. also found that mechanical properties were effectively improved in PU/GO nanocomposite.[38]

In recent times, significant interests in the investigation and development of shape memory polymers (SMPs) are noticed.[39] This is due to their ability to fix in the temporary deformed state and to recover the original shape upon exposure to external stimuli such as a magnetic field, thermal energy, light energy, electric field, etc.[39] On stretching at elevated temperature, the entanglement of the polymer chains of SMPs results in the storage of entropy energy. However, on freezing the molecular motion of the amorphous zone or crystallization of the crystalline zone prevents the molecular chain from reforming a coil-like structure and hence SMPs are fixed in the deformed shape.[40] On further heating of the oriented polymer chains of SMPs, the chains are softened which helps in the regaining of the coiled conformation of the molecular chains. Thus, the driving force for shape recovery in SMPs is elastic energy generated during deformation.[41] In this milieu, HPU exhibited good shape memory behavior due to some interesting features of it such as high recoverable

strain (up to 400%), a wide transition temperature range for its shape recovery, high control of the softening and retraction temperatures, inherent soft–hard segments, favourable and tunable physical properties, etc.[42]

Thus, HPU/GO nanocomposites with three different wt% of GO were prepared in this study. The potential of HPU/GO nanocomposites as shape memory materials was also investigated. The effect of GO on mechanical and thermal properties of the HPU matrix was also studied. The Halpin–Tsai model was used to study the distribution of sheet-like GO in the HPU matrix.

3B.2. Experimental

3B.2.1. Materials

The monoglyceride of the castor oil, TDI, PCL and BD used for the preparation of HPU were same as described in Chapter 2, section 2.2.1. GO was used for the fabrication of nanocomposites, prepared by same procedure as reported in sub-chapter 3A.

3B.2.2. Characterization

FTIR, XRD, DSC and TGA analyses were performed under the same conditions and by using the same instruments as mentioned in Chapter 2, section 2.2.2. Here, the morphology of the nanocomposites was studied by same HRTEM analysis as mentioned in this chapter, section 3A.2.2. A very dilute solution of the nanocomposite was mounted on a carbon coated copper grid and high magnification images were captured. GO was dispersed in DMAc by using an ultrasonicator with same the specification as stated in sub-chapter 3A, section 3A.2.2. Tensile strength, elongation at break, scratch hardness and impact resistance of the nanocomposite were studied by using the same instruments under the same test conditions as mentioned in Chapter 2, section 2.2.2. Halpin–Tsai equations were used to estimate the orientation of the GO sheets in HPU/GO nanocomposites.

$$E_{NC} = E_P \left[\frac{3}{8}\frac{1+\eta_L \zeta V_C}{1-\eta_L V_C} + \frac{5}{8}\frac{1+2\eta_T V_C}{1-\eta_T V_C}\right] \text{---------- (3B.1)}$$

$$E_{\parallel} = E_P \left[\frac{1+\eta_L \zeta V_C}{1-\eta_L V_C}\right] \text{---------- (3B.2)}$$

$$\eta_L = \frac{(E_{GO}/E_P)-1}{(E_{GO}/E_P)+\zeta} \text{---------- (3B.3)}$$

$$\eta_T = \frac{(E_{GO}/E_P)-1}{(E_{GO}/E_P)+2} \text{---------- (3B.4)}$$

where E_P, E_{GO}, E_{NC} and $E_{\|}$, are Young's modulus of HPU, GO, nanocomposites with randomly distributed GO and aligned parallel to the surface of the sample, respectively. ζ and V_C are diameter to thickness ratio and volume fraction of GO, respectively. The density of GO 2.2 g cm^{-3} as reported in literature[43] and the density of PU is evaluated 1.08 g cm^{-3} (Chapter 2, **Table 2.3**). The Young's modulus of GO is adopted 250 GPa according to the measured results.[44]

The shape memory behavior of nanocomposites was investigated through stretching method. At first, films were cut into rectangular strips with the dimension of 4 cm × 1 cm × 0.06 cm and heated at 50 °C for 5 min. Then they were stretched to twice of their original length (L_0) and stretched length was denoted as L_1. Immediately, the stretched samples were frozen by immerging them in ice-salt bath at -5 °C for 5 min to fix the temporary shape and the length was measured as L_2. Subsequently, the samples were reheated at the same temperature (50 °C) for the same period of time for the shape recovery and the length obtained is denoted as L_3. The test was repeated three times.The percentage shape recovery and fixity were calculated by the following equations.

$$\text{Shape recovery (\%)} = \frac{(L_1 - L_3)}{L_0} \times 100 \quad \text{---------- (3B.5)}$$

$$\text{Shape fixity (\%)} = \frac{(L_2 - L_0)}{L_0} \times 100 \quad \text{---------- (3B.6)}$$

3B.2.3. Preparation of HPU/GO nanocomposite

The details of the preparative method of HPU was described in Chapter 2, section 2.2.3.2. For the preparation of nanocomposite, required amount of dispersed GO in DMAc was injected by a syringe after completion of the polymerization reaction at room temperature. After that, the reaction mixture was stirred another 1 h at (70±2) °C to obtain the desired nanocomposite. Finally, the solution of the nanocomposite was cast on inert substrates, followed by vacuum degassed and dried at 50 °C for 24 h for different testing and analyses. The same procedure was followed for the preparation of all three compositions of the nanocomposites. The nanocomposites were coded as HPU/GO0.5, HPU/GO1 and HPU/GO2 for 0.5, 1 and 2 wt% of GO, respectively.

3B.3. Results and discussion

3B.3.1. Characterization of HPU/GO nanocomposite

FTIR was employed to investigate the presence of linkages in HPU/GO nanocomposites. In **Figure 3B.1**, the appearance of characteristic bands of C−N, C–O, C=C, C=O, O–H free, N−

H and C–N stretching and N–H bending vibrations at their position (as mentioned in Chapter 2, section 2.3.2.) clearly indicates the presence of urethane linkage in HPU/GO nanocomposites.[42] The broadening of –OH band was enhanced at 3430 cm^{-1} and C=O band was shifted to 1690 from 1720 cm^{-1} with increasing amount of GO in the nanocomposites. These suggest the presence of strong interaction between HPU and GO in the nanocomposite.[45]

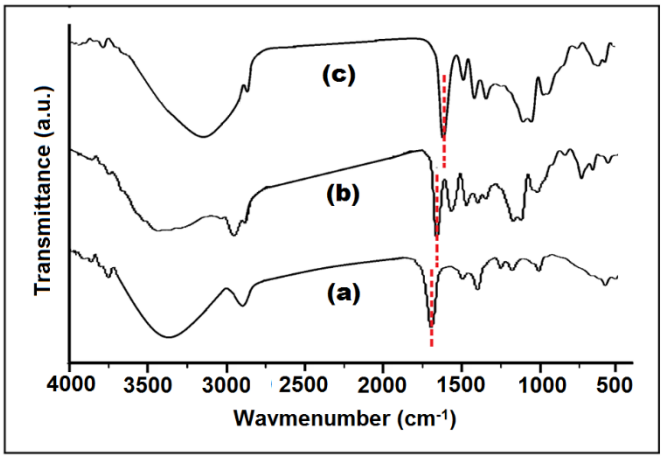

Figure 3B.1 FTIR spectra of (a) HPU/GO0.5, (b) HPU/GO1 and (c) HPU/GO2

The XRD patterns of HPU/GO0.5, HPU/GO1and HPU/GO2 are shown in **Figure 3B.2**. HPU/GO nanocomposites showed two peaks at 2θ = 21.1° (d-spacing = 0.419 nm) and 23.4° (d-spacing = 0.381 nm) for the crystals of PCL moiety.[46] It is noteworthy to note that no peak for GO was found in the nanocomposites. This reflects that no long range order is present in GO sheets, or that the distance between the sheets (caused by the exfoliation of the matrix PU) is too large to provide a signal. In addition to that small amount of GO was used for nanocomposite which may be another reason for this. The peak intensity of PCL moiety also increased with the amount of GO due to the strong nucleating effect of GO and enhancement of the interaction between GO and HPU.[42] In nanocomposites, PCL peaks were little shifted towards higher angle owing to the formation of the dense structure compare to pristine HPU.

The performance of nanocomposites mainly depends on the dispersion of nanomaterials in the polymer matrix and their interfacial interactions.[47] Therefore, to assess the dispersion of GO in the HPU matrix, HRTEM was employed to inspect the morphology of the samples. **Figure 3B.3** shows the HRTEM image of HPU/GO0.5. It can be seen from the image, the exfoliated GO sheets are well dispersed in the matrix of HPU.

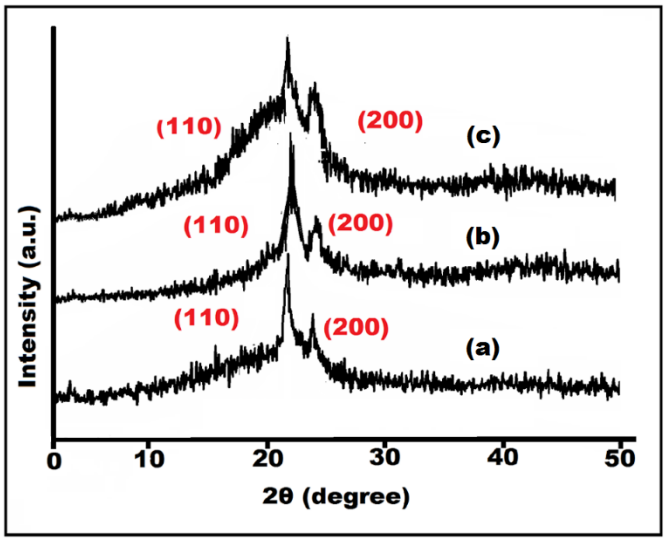

Figure 3B.2 XRD patterns of (a) HPU/GO0.5, (b) HPU/GO1 and (c) HPU/GO2

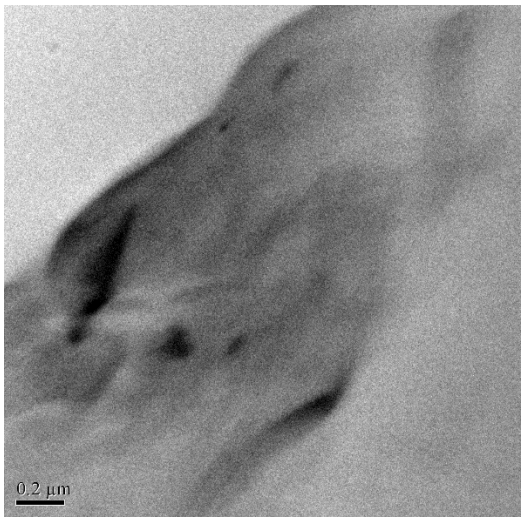

Figure 3B.3 HRTEM micrograph of HPU/GO1

3B.3.2. Mechanical properties of HPU/GO nanocomposite

Figure 3B.4a represents the stress–strain curves of HPU/GO nanocomposites. All the nanocomposites showed nonlinear elastic behavior within the low stress region and high plastic deformation under high stress. All the nanocomposites also exhibited an enhanced elongation at break over the neat HPU. It is a most outstanding feature of the studied nanocomposites. Tensile strength, tensile modulus, elongation at break and toughness of HPU were enhanced to 16 MPa, 5.55 MPa, 810% and 68.07 MJ/m^3 after the incorporation of 2% of GO. The detailed results are tabulated in **Table 3B.1**. The most efficient improvement resulted from the 2 wt% GO, which exhibited increment of 128%, 95% and

167% in tensile strength, elongation at break and toughness, respectively. It indicates that incorporation of GO leads to an effective nanocomposite, and the resistance to mechanical deformation can be reinforced along with the enhancement of the elongation of the nanocomposites. Better mechanical properties such as tensile modulus and strength for the HPU/GO nanocomposites could be due to good interfacial interaction upon uniform dispersion of GO in the HPU matrix.[43] There is also a possibility of direct linkages between various oxygenating groups of GO and HPU chains by physico-chemical interactions. This greatly enhances the compatibility of GO with the HPU matrix. Thus, it becomes favourable to transfer stress to GO, which improves the mechanical strength of the nanocomposite. The presence of an immobilized or partially mobilized polymer phase, as a consequence of such interactions, and orientation of GO and the polymer chain along the direction of tensile flow, provides a great contribution to the observed enhancement of the tensile strength.[47] Further, with an increment of GO amount, the surface area of such nanomaterials increases which enhances the above factors and thereby improving the mechanical properties.

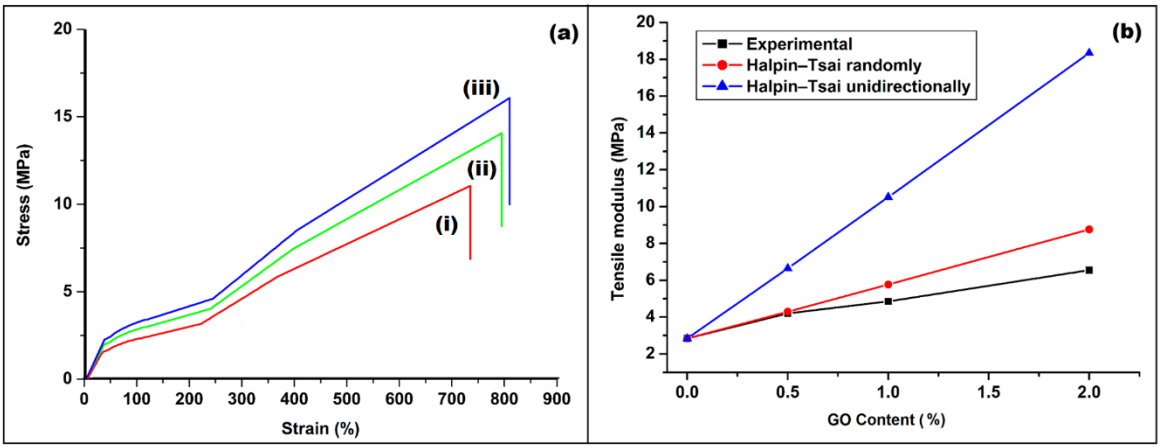

Figure 3B.4 (a) Stress-strain curves of (i) HPU/GO0.5, (ii) HPU/GO1 and (iii) HPU/GO2, and (b) comparison between the fitting results from the Halpin–Tsai model and the experimental data

Elongation at break enhances with the increased of the amount of GO in the nanocomposites. This enhancement of the elongation at break by the formation of nanocomposite is due to the slippage of the graphene layers when they are attached to the polymeric chains.[43] In addition, the immobilized or partially mobilized chains are able to extend fully, and thus a good enhancement of elongation was observed.[43]

The Halpin–Tsai equation was used to estimate the orientation of the GO sheets in the nanocomposites.[47] In order to understand it, the Young's moduli of the HPU nanocomposites are calculated and compared with the experimental results with different GO orientations, as shown in **Figure 3B.4**b. It is cleared that the 3-dimensional random model shows a better fit to the experimental results compared with the 2-dimensional aligned model, particularly at low GO content. This indicates that the GO is randomly distributed in the HPU matrix. The deviation of modulus value gradually enlarged on increasing the GO content. As their Young's moduli are obtained from the linear area of the stress–strain curves (in general lower than 20% strain), alignment of GO along the load direction is restricted. Especially for the low GO containing nanocomposite, e.g., 0.5 wt%, there is adequate space in the nanocomposite which permits GO to arrange in a random manner. With the increased of GO content, such space reduces and the interaction between adjoining GO forces them to align along the force direction, resulting in enlarged deviation to the prediction of the random model.[43] The scratch hardness of the pristine HPU and its nanocomposites are given in **Table 3B.1**. After incorporation of GO in the HPU matrix scratch hardness is enhanced which further suggests that the toughness of the material increases. As HPU possesses both aromatic and aliphatic moieties with unique structural architecture, it exhibited high toughness, scratch hardness and impact resistance.[40] Further, HPU absorbed the highest limit of impact energy due to the presence of soft segments which dissipate the impact energy by the segmental motions in its molecular chains.[42]

Table 3B.1. Mechanical properties of HPU and HPU/GO nanocomposite

Property	HPU[#]	HPU/GO0.5	HPU/GO1	HPU/GO2
Tensile strength (MPa)	7.06 ±0.3	11.23± 2.2	14.05±2.8	16.11±3.1
Tensile modulus (MPa)	2.84±0.2	4.2±0.25	4.85±0.37	6.55±0.32
Elongation at break (%)	695±43	735±57	795±36	810±46
Toughness (MJm^{-3})	25.4±1.28	42.47±1.64	58.45±1.08	68.07±2.11
Scratch hardness (kg)	5±0.2	5.5±0.1	5.5±0.2	6.5±0.2
Impact strength (cm)	>100	>100	>100	>100

[#]As reported in Chapter 2, Table 2.3

3B.3.3. Thermal properties of HPU/GO nanocomposite

It is reported that the nanomaterials can influence the melting and the crystallization behavior of HPU.[42] Therefore, DSC analyses were carried out to investigate the crystallization and melting behavior of HPU/GO nanocomposites. Thermal properties of HPU/GO nanocomposites, such as T_g and T_m, were determined from each DSC curve. **Figure 3B.5** clearly shows that T_g increases from 20.3 °C to 22.3 °C and T_m increases from 48.1 °C to 50.7 °C upon incorporation of 2 wt% GO. The small increment in T_g and T_m are due to the presence of GO, which may inflict restrictions on molecular mobility at earlier stages. This influence depends on the interactions of GO bonding with the surrounding HPU matrix. Thermal measurements also illustrate that the crystallization behavior is significantly changed with loading of GO as compared to the pristine HPU (**Table 3B.2**). The amount of crystallinity was calculated from the enthalpy data of the crystalline melting peak. This clearly reflects that GO serve as the nucleating agents in this system and the presence of GO can enhance the crystallization process by inducing the polymer chains in a particular direction.[45]

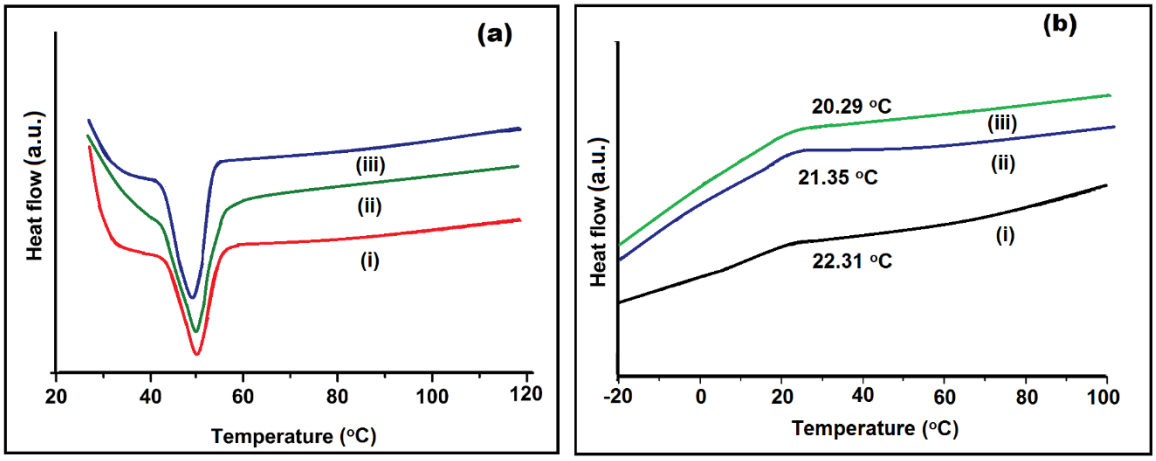

Figure 3B.5 DSC curves showing the (a) T_m (heating cycle) and (b) T_g (cooling cycle) of (i) HPU/GO2, (ii) HPU/GO1 and (ii) HPU/GO0.5

To verify the thermal stability of HPU/GO nanocomposites, TGA was performed. HPU/GO nanocomposites also exhibited two steps degradation (**Figure 3B.6**) similar to pristine HPU. This is suggested that degradation mechanism of HPU did not influence by the incorporation of GO. The degradation temperature of the nanocomposites was only shifted to higher temperature compared to that of pristine HPU (Chapter 2, section 2.3.8). The thermal stability of HPU was improved after incorporation GO, although GO itself is a thermally unstable. The enhanced thermo-stability of the nanocomposites with loading of

the GO is due to restricted motion of the polymeric chains. This restriction is arisen from the different physicochemical interactions with GO.[45] The volatiles generated during the decomposition were retained longer time in the matrix due to improved barrier characteristics.

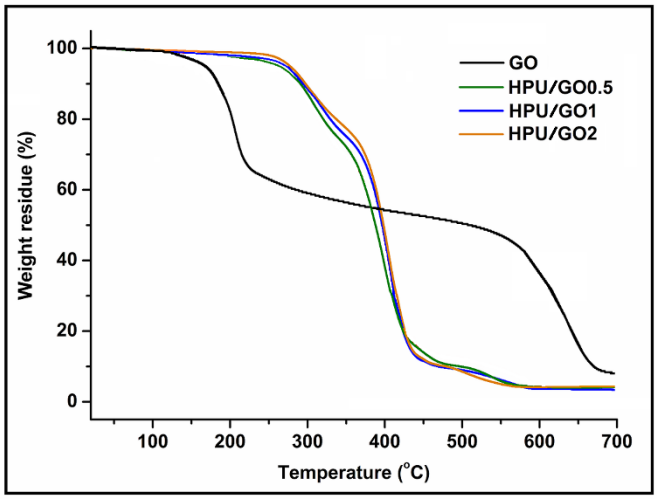

Figure 3B.6 TGA thermograms of GO, HPU/GO0.5, HPU/GO1 and HPU/GO2 [TGA thermogram of GO are used from sub-chapter 3A for better comparison]

3B.3.4. Shape memory behavior of HPU/GO nanocomposite

The shape memory behavior and possible molecular mechanism of shape memory behavior of HPU and HPU/GO nanocomposites are shown in **Figure 3B.7**. The shape memory behavior of a material mainly depends on two fundamental factors (i) occurrence of a quantitative amount of unlocked orientated polymer chains and (ii) the modulus at room temperature. All polymeric chains experience the same level of deformation when an external force is applied to stretch the sample.[48] The produced deformation is memorized by crystallization or orientation of the soft segment. However, the 'unlocked' chains, the chain segments which do not crystallize generate an instantaneous retractive force upon removal of the tensile load due to the entropy of elasticity. Nevertheless, this retractive force alone is insufficient to an instantaneous recovery of the shape as the fraction of mobile chains is usually low. The instantaneous retractive force can cause only limited instantaneous recovery strain if the room temperature modulus is high.[42] On the other hand, a more rapid recovery occurs if the value of the modulus is low. Switching temperature was selected as 50 ^{o}C which was close to the T_m to obtain the best results. As melting transition is sharper

transition compared to the glass transition and at the melting temperature stretching of HPU is also facilitated.[40]

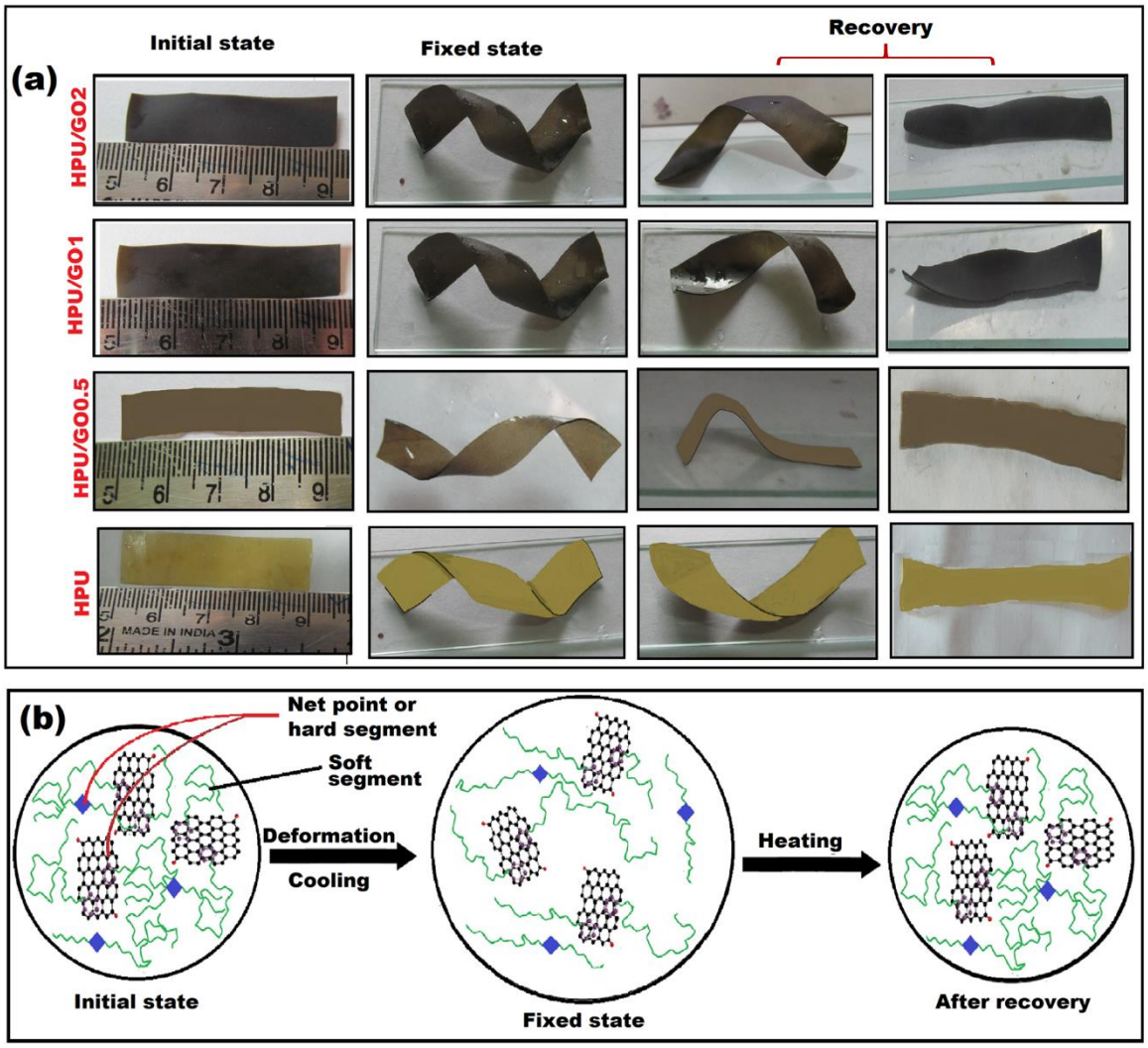

Figure 3B.7 (a) Shape memory behavior of HPU and HPU/GO nanocomposites, and (b) possible molecular mechanism of shape memory behavior

The nanocomposites exhibited excellent shape memory behavior on the incorporation of GO as shown in **Table 3B.2**. This can be explained by the increased stored energy as a result of homogeneously distributed GO in HPU matrix, which increased the interaction between GO sheets and hard segment of HPU, mainly by π-π stacking and generated strong net points.[42] Thus, GO created high stored elastic strain energy, which in turn helped the nanocomposites to gain high recovery stress due to release of stored elastic strain.[49] The shape recovery was also found to increase with an increased amount of GO in the matrix. It may be justified to correlate the enhanced degree of crystallinity to this

escalating trend of shape recovery.[42] The augmented crystallinity on the incorporation of GO (as obtained from DSC and XRD results) resulted in the increased tendency to generate more amount of unlocked oriented chains. These unlocked chains can generate an instantaneous retractive force upon elimination of the load because of the elastic entropy and hence it improved the shape recovery.[49]

Table 3B.2 T_m, crystallinity and shape memory behavior of HPU and HPU/GO nanocomposite

Sample	T_m (^oC)	Crystallinity (%)	Shape fixity (%)	Shape recovery (%)
HPU	48.1*	25.88*	93.3±1.4	88.8±1.1
HPU/GO0.5	49.3	32.53	92.1±1.1	93.5±1.4
HPU/GO1	50.2	36.68	90.8±1.1	94.6±0.6
HPU/GO2	50.7	38.79	90.1±1.8	96.3±0.2

* As reported in Chapter 2, Table 2.4

3B.4. Conclusion

From this study, it can be concluded that a large scale production of highly stretchable castor oil based HPU reinforced GO nanocomposites is possible through the studied route. The nanocomposites can exhibit excellent toughness along with enhancement of flexibility in addition to other mechanical properties on incorporation of GO. Halpin-Tsai model fitting suggests 3D random distribution of GO in the HPU matrix. It can be concluded that the overall shape recovery of the nanocomposite, (to the extent of 96.3%) is quite significant compare to the pristine HPU. Thus, this investigation showed a strong influence the GO on the performance of HPU.

3C. Preparation of HPU/reduced graphene oxide nanocomposite

3C.1. Introduction

The previous sub-chapter described the potential of GO as a nanoreinforcing agent to improve various properties such as mechanical, thermal and especially shape memory behavior of pristine HPU. However, the shape memory effects by direct heating are the most common and usual, other stimuli such as light, magnetic and microwave (MW) gradually become attractive at present.[39] This is as a consequence of the capability to utilize reduced operating temperatures, be applied remotely, and result in localized shape-memory effects. Generally, light-induced shape-memory is attained either via light-induced heating or through photochemistry.[39] For example, Lendlein and co-workers used UV light as a stimulus to enable shape-memory effects by way of a photo-reversible cyclo-addition reaction.[50] Magnetic field induced SMP is generally obtained by incorporating magnetic particles in the SMP matrix. The incorporation of the particle improved the mechanical properties as well as enabled to generate the shape memory effect under an alternating magnetic field.[39] In addition, MW is also an alternative choice as a noncontact stimulus for shape recovery of SMP. Recently Kalita and Karak reported that PU/iron oxide nanocomposite exhibited excellent shape recovery under the MW power.[40] Even though remote shape-memory effects are developed using IR or UV irradiation, magnetic field, MW, etc. as the stimuli; but most of the polymer are poorly responded under such stimuli due to the low thermal conductivity of these materials. Therefore, good thermal conductive nanomaterials are required to improve uniform heat transfer ability to the SMP matrix and thereby facilitating efficient remote heating.[51] In this milieu, graphene is the most attractive material for the above purpose as it has excellent thermal conductivity, electrical conductivity, MW absorbing capacity, light absorbing ability including sunlight and so forth.[1,3,52,53]

However, homogenous dispersion of graphene in the polymer matrix is one of the paramount factors as aggregation or restacking of graphene sheets commonly occurs in most of the cases because of the π–π stacking and hydrophobic interactions among the sheets.[54] Again the weak interactions between graphene and polymeric matrix result in interfacial slippage on application of external stress, limiting the improvement of mechanical properties.[55] Although functionalization is a promising way to improve dispersibility and interaction of graphene with polymer matrix, but such functionalization of graphene is difficult due to its inertness.[56] Even though, GO possesses good dispersibility and

compatibility with polar HPU as described in previous sub-chapter, HPU/GO nanocomposites are electrically insulating in nature as GO itself is electrically insulating nanomaterial. In this context, reduced GO (RGO) exhibits almost similar in chemical structure and properties with graphene.[1] It contains some residual oxygenating groups which further help to disperse in HPU matrix and it can be easily functionalized.[31] Thus, it is a right choice to develop a shape memory HPU nanocomposite which can be triggered by microwave and sunlight along with thermal energy.

Therefore, in this present investigation, an effective technique was demonstrated to fabricate HPU nanocomposites using RGO or functionalized RGO (f-RGO) as a reactive chain extender as well as a reinforcing nanomaterial, at different wt%. This *in situ* generated HPU nanocomposites were characterized by FTIR, XRD, DSC and TGA analyses. The performance including mechanical and electrical properties of the nanocomposites as well as multi-stimuli responsive shape memory behavior under thermal, MW and sunlight was also delved into.

3C.2. Experimental

3C.2.1. Materials

The monoglyceride of the castor oil, TDI, PCL and BD used for the preparation of HPU were same as described in Chapter 2, section 2.2.1. The same RGO (reduced by *C. esculenta* leaf extract) was used for the fabrication of nanocomposites as reported in sub-chapter 3A.

3C.2.2. Characterization

FTIR, XRD, DSC and TGA analyses, and mechanical tests were performed under the same conditions and by using the same instruments as described in Chapter 2, section 2.2.2. Functionalization of RGO and distribution of RGO in the prepared nanocomposite were analyzed by using the same HRTEM analysis as mentioned in Chapter 3, section 3B.2.2. The conductivity of the polymer films was measured by using Hioki-3532-50 LCR Hitester instrument. Film sample (20 mm in diameter with 0.5 mm thickness) were loaded between the two circular electrodes of the device and tested under ambient conditions.

Thermo-responsive shape memory test was performed by same procedure as mentioned in the previous sub-chapter, section 3B.2.2. To study the shape memory behavior under MW and direct sunlight, the bending test was performed. A domestic microwave oven (800 W) operating at a frequency of 2.45 GHz was used for the test. The samples were folded

in a ring form at 60 °C followed by quenching into an ice-salt bath for 5 min at -10 °C. Then the shape recovery of the nanocomposite films was achieved by exposing MW irradiation of 360 W for 30-60 s and direct sunlight (11 am-2 pm, at Tezpur University campus, altitude: 26.63 °N 92.8 °E in the month of March at sunny days, average temperature 34±1 °C and humidity 74±1 %) under ambient condition. The shape recovery was calculated using the following equation.

$$\text{Shape recovery} = \frac{(90-\theta)}{\theta} \text{ ---------- (3C.1)}$$

where θ in degree denotes the angle between the tangential line at the midpoint of the sample and the line connecting the midpoint and the end of the curved samples.

3C.2.3. Functionalization of RGO

The amount of reactive hydroxyl groups on RGO was 0.58 mmol/g as measured by titration of the excessive isocyanate groups using butyl amine. The excess isocyanate was determined after reacting RGO with a known amount of TDI at 70 °C. On the basis of the above result, functionalization on RGO sheets was done by reacting with a required amount of TDI followed by BD. Briefly, 2 g of RGO was dispersed in 100 mL of distilled THF by mechanical stirring for overnight followed by 15 min ultrasonication. This dispersed RGO was taken in a three-necked round bottom flask equipped with a mechanical stirrer, nitrogen inlet and rubber septum. Then, 0.5 mmol of TDI was added drop wise into the reaction mixture at room temperature by the help of a syringe through the septum. The reaction was continued for 4 h at a temperature of (70±2) °C to obtain isocyanate terminated RGO. Then, 0.5 mmol of BD was added drop wise into the mixture, and the reaction was continued for another 1 h to obtain the desired f-RGO. This f-RGO was centrifuged and washed with THF to separate the free reactants. The f-RGO was dried in a vacuum oven at 45 °C for overnight prior to use.

3C.2.4. Preparation of HPU/RGO and HPU/f-RGO nanocomposites

HPU/RGO and HPU/f-RGO nanocomposites were prepared following the same method which was used to prepare HPU in Chapter 2, section 2.2.3.2. Only required amount of dispersed RGO or f-RGO in DMAc (different wt%: 0.5, 1 and 2 with respect to total weight of nanocomposite) was incorporated in 1st step of the polymerization reaction to get *in situ* nanocomposites. Then, the reaction was continued for 3 h at temperature of (70±2) ºC to

obtain the desired viscous mass, which was treated as the pre-polymer. After that, 2nd step of the polymerization was carried out at (110±2) ºC for 2.5 h.

HPU with 0.5, 1 and 2 wt% of f-RGO were encoded as HPU/f-RGO0.5, HPU/f-RGO1 and HPU/f-RGO2, respectively, and HPU with 0.5, 1 and 2 wt% of RGO were encoded as HPU/ RGO0.5, HPU/ RGO1 and HPU/ RGO2, respectively.

3C.3. Results and discussion

3C.3.1. Functionalization of RGO

The functionalization was achieved by reacting the isocyanate groups of TDI with the residual oxygenated functional groups of RGO sheets to obtain isocyanate terminated RGO sheet, followed by reacting with BD. Stable dispersion of f-RGO even after 2 months of storage in various solvents such as THF, DMF, DMSO and DMAc was observed as shown in **Figure 3C.1**.

Figure 3C.1 Dispersion stability of f-RGO in different solvents after 2 months of storage

3C.3.2. Characterization of f-RGO

The functionalization of RGO was characterized by FTIR, XRD and TEM analysis. FTIR spectra of RGO, isocyanate terminated RGO and f-RGO are shown in **Figure 3C.2**a. The presence of urethane linkage in the FTIR spectrum of the intermediate (before adding BD) indicates the reaction of TDI with available hydroxyl groups of RGO. In the spectra of the intermediate product (isocyanate terminated RGO) and f-RGO, two new bands appeared in the ranges of 2800–2880 and 2880-3000 cm^{-1} which are assigned to the symmetric and asymmetric C-H stretching vibrational bands.[45] More direct evidence was obtained from the absorption at 1701, 1646, 1219, 1054 and 1543 cm^{-1} appeared in the spectra of both, which are attributed to the stretching vibration of carbonyl of amide I, C=C, C-O, C-N and bending of N-H of amide II of urethane linkage respectively.[40,42] This analysis indicates the validity of the covalent bond formation with RGO.

RGO shows a broad peak centered at 2θ = 25° corresponding to d-spacing of 0.36 nm for the d_{002} plane in the XRD pattern (Chapter 3, section 3A.3.4). After functionalization of RGO, this peak was shifted to the lower angle (2θ = 21.2° corresponding to d-spacing of 0.415 nm), which indicates that the d-spacing between the layers was increased due to the presence of urethane chains (**Figure 3C.2**b).[40]

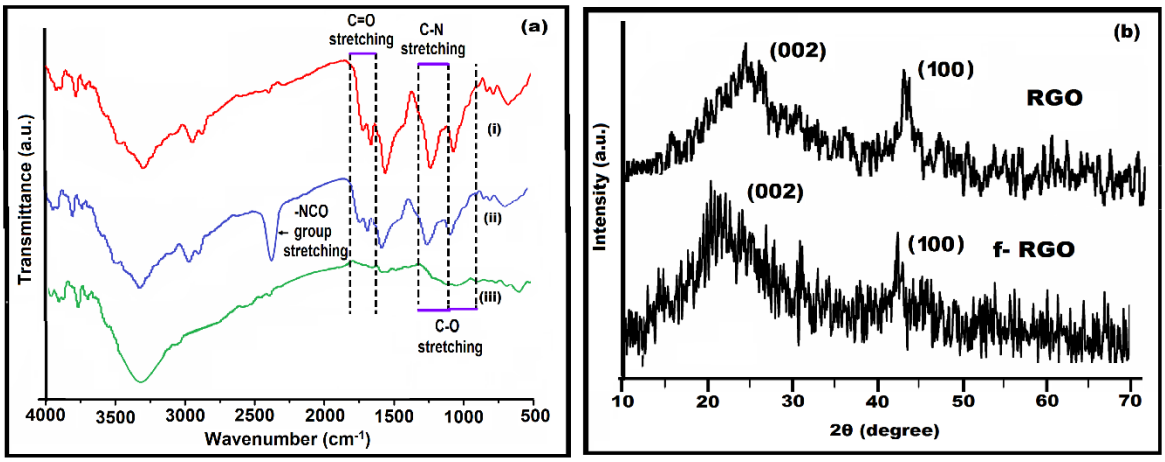

Figure 3C.2 (a) FTIR spectra of (i) f-RGO, (ii) isocyanate-terminate RGO and (iii) RGO; and (b) XRD patterns of f-RGO and RGO [FTIR spectrum and XRD patterns of RGO are used from sub-chapter 3A for better comparison]

HRTEM image of f-RGO are shown in **Figure 3C.3**a. More folds or wrinkles were found after the functionalization of RGO compared to pristine RGO (Chapter 3, section 3A.3.6). The enhancement of the amorphous nature of RGO after functionalization was further confirmed by SAED patterns (**Figure 3C.3**b).

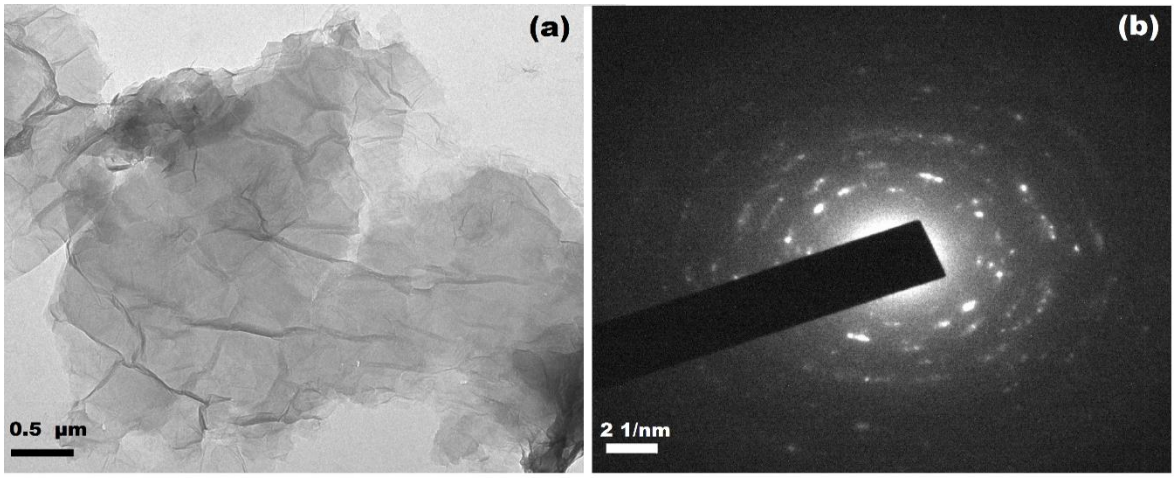

Figure 3C.3 HRTEM image of (a) f-RGO and (b) SAED patterns of f-RGO

3C.3.3. Characterization of HPU/RGO and HPU/f-RGO nanocomposites

FTIR spectra of HPU/f-RGO0.5, HPU/RGO0.5, HPU/f-RGO2 and HPU/RGO2 are shown in **Figure 3C.4**. The appearance of characteristic bands of C−N, C–O, C=C, C=O, O–H free, N−H, C−N stretching and N−H bending vibrations at their positions clearly indicates the presence of urethane linkage (as mentioned in Chapter 2, section 2.3.2.).[40,45] The increase in broadening of –OH band and shifting of C=O band were observed with the increasing amount of f-RGO or RGO in the nanocomposite similar to HPU/GO nanocomposite as described in previous sub-chapter. These confirm the presence of different interactions among the HPU chains and RGO or f-RGO, which are enhanced with the nanomaterial content.[45]

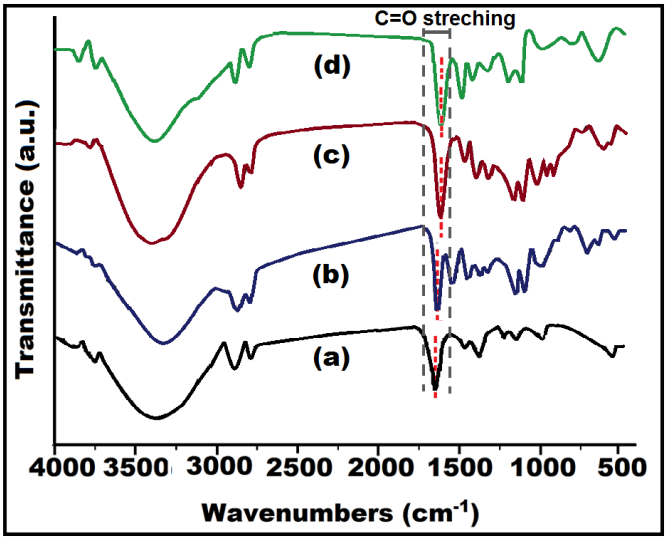

Figure 3C.4 FTIR spectra of (a) HPU/RGO0.5, (b) HPU/f-RGO0.5, (c) HPU/RGO2 and (d) HPU/f-RGO2

The XRD patterns of HPU nanocomposites showed two peaks at 2θ = 21.1° and 23.4° for the crystals of PCL moiety of HPU in **Figure 3C.5**(i).[42] Here it is important to mention that no separate peak was observed for RGO or f-RGO in the nanocomposites similar to HPU/GO nanocomposite. This may be due to the presence of a small amount of nanomaterial in the nanocomposite. In the nanocomposites, PCL peaks were slightly shifted towards higher angle owing to formation of the dense structure compared to the pristine HPU.[42] Also, the peak intensity of the PCL moiety marginally increased with an increase in the amount of nanomaterial due to the nucleating effect of nanomaterial. **Figure 3C.5**(ii) shows the HRTEM image of HPU/f-RGO1. It can be seen from **Figure 3C.5**(ii) the exfoliated f-RGO sheets are well dispersed in the matrix of HPU.

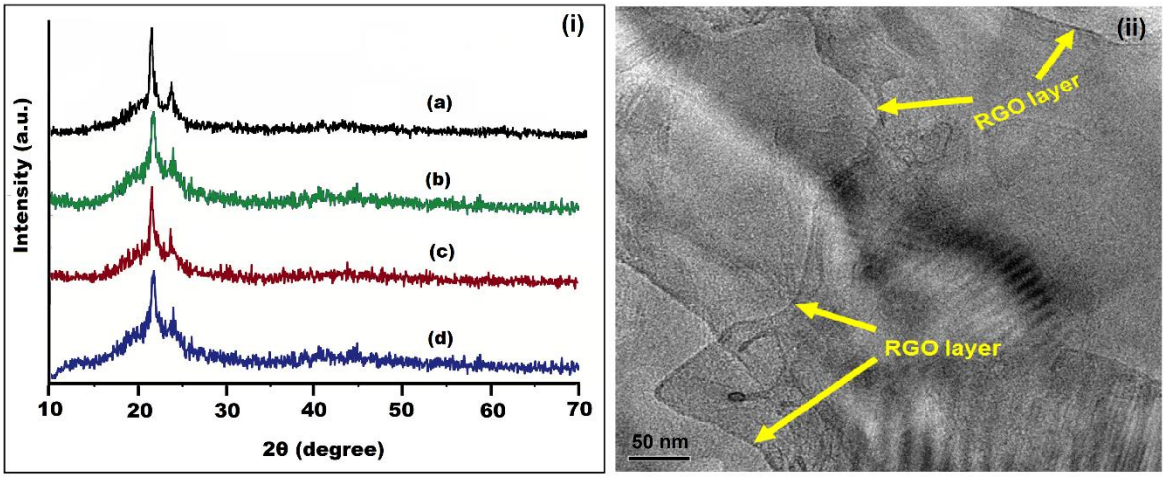

Figure 3C.5 (i) XRD patterns of (a) HPU/RGO0.5, (b) HPU/f-RGO0.5, (c) HPU/RGO2 and (d) HPU/f-RGO2; and (ii) HRTEM micrograph of HPU/f-RGO1

3C.3.4. Mechanical properties of HPU/RGO and HPU/f-RGO nanocomposites

An extensive enhancement in the mechanical properties of the *in situ* generated nanocomposites is due to the existence of covalent bonding between RGO or f-RGO and isocyanate terminated pre-polymer. This helps to form strong interfacial interaction between HPU chain and homogeneously dispersed nanomaterial. The values of tensile strength, tensile modulus, toughness and elongation at break of HPU/RGO and HPU/f-RGO nanocomposites with different loadings of RGO and f-RGO are tabulated in **Table 3C.1** and the typical stress-strain profiles are shown in **Figure 3C.6**. All the nanocomposites showed dose-dependent mechanical property as noticed in case of HPU/GO nanocomposites. Tensile modulus and toughness were enhanced enormously after the formation of nanocomposite with 2 wt% of f-RGO. HPU/f-RGO nanocomposites exhibited superior mechanical properties compared to the respective HPU/RGO nanocomposites. This confirmed the presence of stronger interactions with homogeneous distribution of f-RGO in HPU/f-RGO nanocomposites than with RGO in HPU/RGO nanocomposites. Although, HPU/RGO nanocomposites demonstrated better mechanical properties than corresponding HPU/GO nanocomposite (**Table 3B.1**).

Such superior mechanical properties can certainly be ascribed to the strong interfacial adhesion and good compatibility between RGO or f-RGO and HPU matrix.[47] The hard domain of HPU is stiffened due to the presence of strong covalent bond between RGO or f-RGO and HPU chains.[57] For this reason, the resulted nanocomposites exhibited such unusual improvement in tensile modulus (**Figure 3C.6**). In addition to that, the high strength

indicates the preferential orientation of the rigid RGO or f-RGO in the matrix at high strains and hence synergistic effect was observed. This contributes to the dramatic enhancement of modulus.[43]

Table 3C.1 Mechanical properties of HPU/RGO and HPU/f-RGO nanocomposites

Property	HPU/f-RGO0.5	HPU/f-RGO1	HPU/f-RGO2	HPU /RGO0.5	HPU /RGO1	HPU /RGO2
Tensile strength (MPa)	25.6±1.3	33.4 ±2.1	37.6 ±1.8	17.6 ±1.5	24.8 ±1.6	27.8±1.9
Tensile modulus (MPa)	22.4±0.4	101.8 ±3.4	128.5 ±4.2	12.4 ±1.2	25.3 ±1.1	36.3±3.2
Elongation at break (%)	1256±50	1432±32	1656±43	890±28	940±46	980±34
Toughness (MJm^{-3})	107.9 ±4.3	348.16 ±5.1	454.82 ±6.2	63.72 ±2.1	96.34 ±3.4	115.78 ±4.1
Scratch hardness (kg)	6.5±0.1	7±0.1	7.5±0.1	5.5±0.2	6±0.2	6.5±0.1
Impact strength (cm)	>100	>100	>100	>100	>100	>100

Interestingly, elongation at break of RGO based HPU nanocomposites was also found to increase compared to pristine HPU (Chapter 2, Table 2.3). This is the most protuberant feature of these nanocomposites. Although, the addition of graphene generally aids an enhancement of tensile modulus value, but the elongation at break always shows complex behavior with graphene content in PU nanocomposites. For example, Wu et al. found a continuous decreased in elongation at break with the increase of the graphene content.[58] In addition, the experimental results by Chen et al. showed the nanocomposites retain almost identical elongation at break to that of the pristine PU.[43] In contrast, fabricated HPU/f-RGO nanocomposite showed an interesting and very useful mechanical behavior. A simultaneous enhancement of elongation at break along with the improvement of tensile strength, tensile modulus and toughness values was observed. Such anomalous results are due to a full extension of the covalently and non-covalently bonded HPU chains.[43] Also, HPU chains are aligned in the initial stage of tensile loading which forced to orient f-RGO

along the loading direction.[57] At high stress, layers of f-RGO are sliding each other due to the presence of strong covalent bonds as well as multiple H-bonding between f-RGO and the adjacent HPU chains.[43] This helps to overcome the π-π stacking interactions among f-RGO sheets. As f-RGO preferentially reinforced the hard segments rather than soft segments that avoided the unusual stiffness of soft segments.[57] This combined effect results such enhancement in the elongation at break of the nanocomposites which was not achieved so far. HPU/RGO nanocomposite also exhibited a better elongation at break compared to pristine HPU and HPU/GO nanocomposite but much lesser than HPU/f-RGO nanocomposite. As, RGO contains a few number of hydroxyl groups on its surface and it was incorporated in the 1st step of the polymerization technique, there is a chance to react some of these hydroxyl groups of RGO with isocyanate groups and form a few strong covalent bonds (urethane linkages).

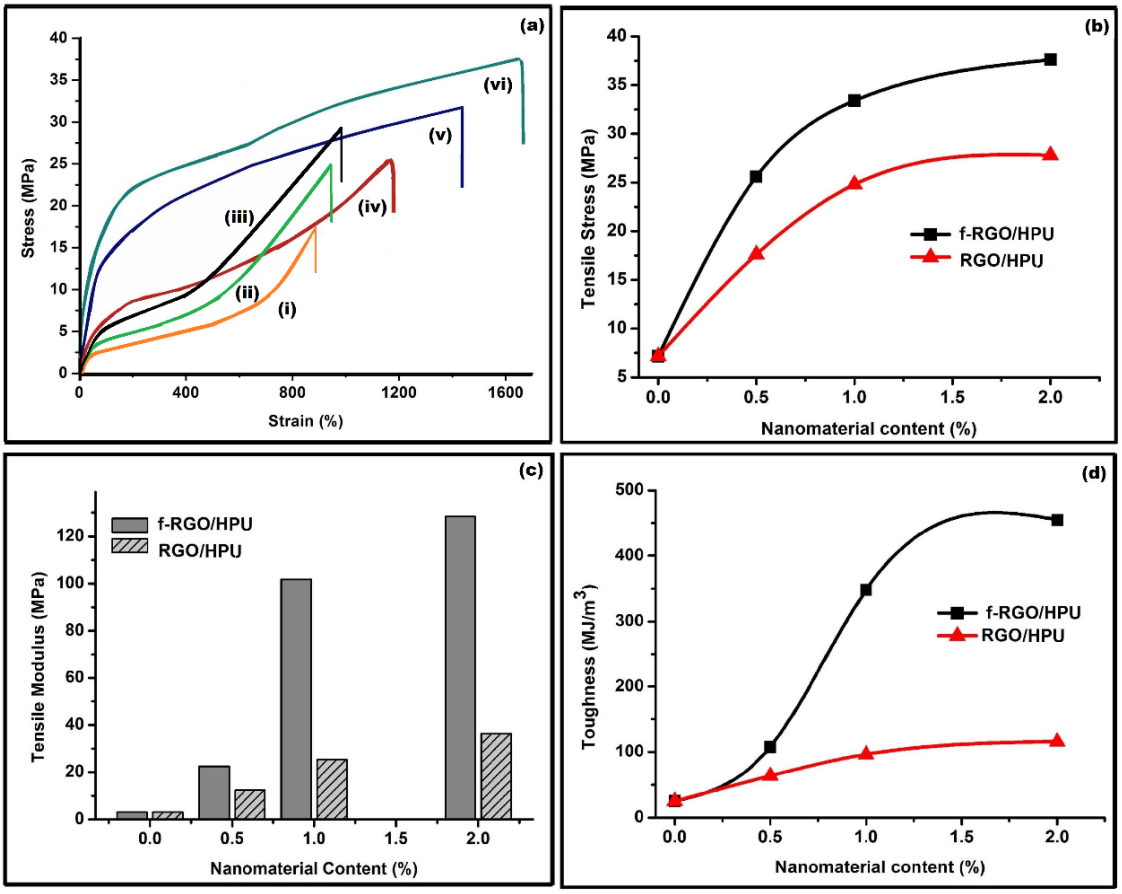

Figure 3C.6 (a) Stress−strain profiles of (i) HPU/RGO0.5, (ii) HPU/RGO1 and (iii) HPU/RGO2 (iv) HPU/f-RGO0.5, (v) HPU/f-RGO1 and (vi) HPU/f-RGO2; and (b) tensile stress, (c) tensile modulus, and (d) toughness of HPU/f-RGO and HPU/RGO nanocomposites at different wt% of nanomaterial

It is quite obvious that the toughness of the nanocomposite is also enhanced as it is the combined effect of strength and flexibility. To find out the reason behind such huge enhanced in mechanical properties we take help of toughening mechanism of bio-composites. The toughness of nanocomposites originate from secondary "sacrificial" bonds between coiled polymeric chains.[43] These sacrificial bonds are ruptured instead of the primary covalent bonds present in nanocomposites under the applied stress. This allows long hidden lengths to loosen and dissipate significant amounts of energy by maintaining structural integrity to large strains. The weak interlayer interactions of f-RGO may also overcome without damaging the integrity of the structure of sheets under the applied stress in the nanocomposites to dissipate significant amounts of energy and hence enhanced toughness was obtained.[43] The H-bond interaction between hydroxyl groups of f-RGO and urethane chains mainly transferred most of the applied stress during the sliding of f-RGO layers (sacrificial bond rupture). Further increase in the applied load finally causes the dissociation of these H-bonds (hidden length release). This enables the nanocomposite to enhance the inherent flexibility of the pristine HPU and to exhibit the high ductility. The plausible toughening mechanism is shown in **Scheme 3C.1**. Both the flexibility and ductility of nanocomposites are largely reliant on the mobility of polymer segments and f-RGO.[59]

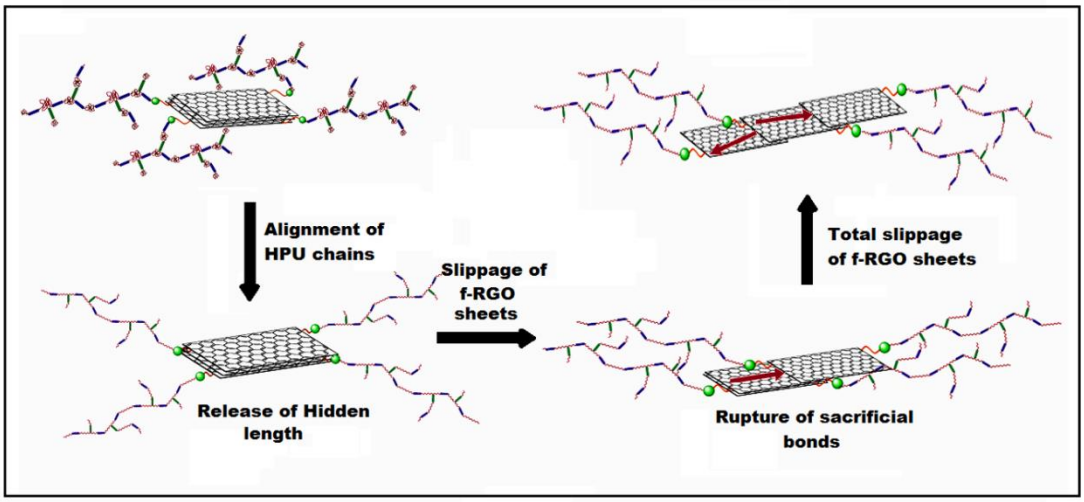

Scheme 3C.1 Possible mechanism of high elongation at break and toughness of HPU/f-RGO nanocomposite

The mobility of f-RGO and polymer segments was diminished as some f-RGO were bonded with HPU. This aids the load transfer between soft and hard segments. In contrast, generation of sacrificing bonds and hidden lengths at the interfaces of nanocomposites

provides an effective resolution to balance the strength, toughness and ductility.[43] It enables one to not only control the mobility of f-RGO in HPU matrix but also ensures efficient load transfer at the interfaces. The introducing such biomimetic interfaces may expose a new hopeful arena for the development of high-performance nanocomposites.

3C.3.5. Thermal properties of HPU/RGO and HPU/f-RGO nanocomposites

After incorporation of 2 wt% RGO and f-RGO in HPU, T_m was increased from 48.4 °C to 51.2 °C and 51.6 °C, respectively as shown in **Figure 3C.7**. Such small increment of T_m is due to restriction of molecular mobility of HPU chains by nanomaterial at the initial stage of heating as mentioned in case of HPU/GO nanocomposites.[40] The degree of crystallinity of the studied nanocomposites are tabulated in **Table 3C.2**. The degree of crystallinity reflects that RGO and f-RGO show positive effect on the crystallization process of the nanocomposites.

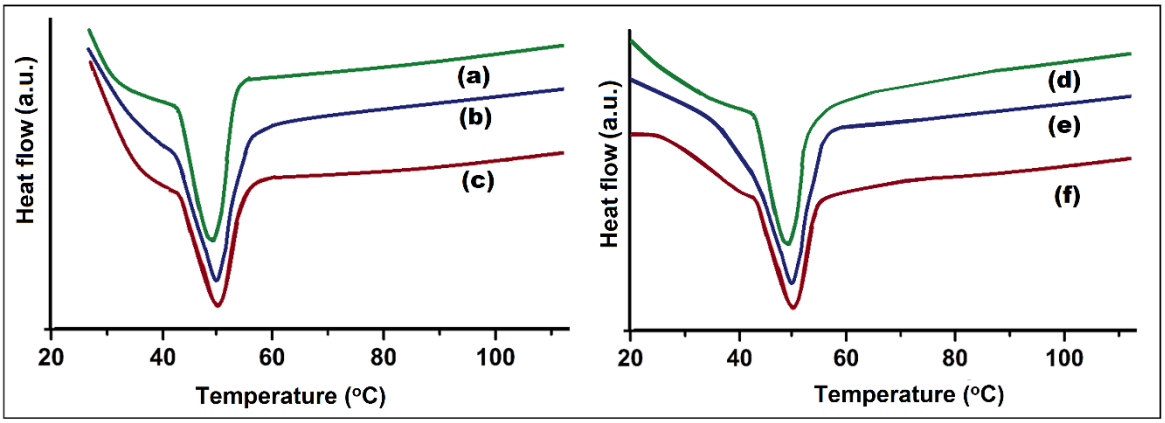

Figure 3C.7 DSC curves of (a) HPU/f-RGO0.5, (b) HPU/f-RGO1, (c) HPU/f-RGO2, (d) HPU/RGO0.5, (e) HPU/RGO1 and (f) HPU/RGO2

Table 3C.2 Thermal properties of HPU/RGO and HPU/f-RGO nanocomposites

Property	HPU/f-RGO0.5	HPU/f-RGO1	HPU/f-RGO2	HPU /RGO0.5	HPU /RGO1	HPU /RGO2
T_m (°C)	49.5	51.1	51.6	49.3	50.8	51.2
Crystallinity (%)	33.15	37.14	39.25	32.46	36.75	38.63

TGA was performed to verify the thermal stability of HPU/RGO and HPU/f-RGO nanocomposites (**Figure 3C.8**). All the nanocomposite exhibited two steps degradation patterns similar to HPU/GO nanocomposite. HPU/f-RGO exibitted higher degradation temperature compared to that of HPU/RGO nanocomposite with same nanomaterial content. The enhanced thermo-stability of the nanocomposites with loading of RGO or f-RGO is due to the same reason as mentioned in HPU/GO nanocomposites (sub-chapter 3B, section 3B.3.3). As, physic-chemical interactions are more in HPU/f-RGO nanocomposite than HPU/RGO nanocomposite, it has higher thermal stability.[40]

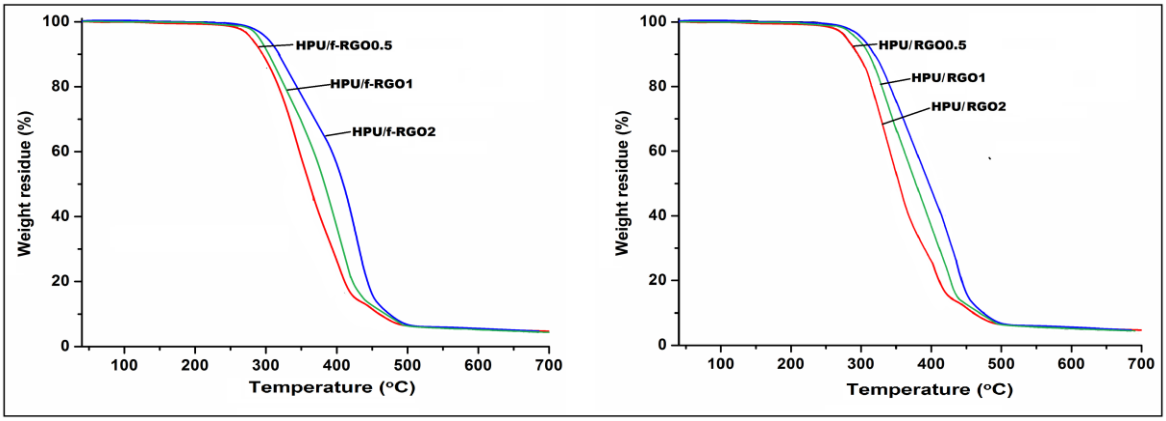

Figure 3C.8 TGA thermograms of HPU/RGO and HPU/f-RGO nanocomposites

3C.3.6. Electrical properties of HPU/RGO and HPU/f-RGO nanocomposites

Figure 3C.9 depicts the electrical conductivity values of HPU, HPU/RGO and HPU/f-RGO nanocomposites. The variation of conductivity as a function of nanomaterial content is shown in this figure. It was observed that the conductivity increased exponentially at low RGO or f-RGO content, followed by a slow growth at the high content. The electrical conductivity was jumped by almost 10 order of magnitude from 10^{-11} to 0.16 S by incorporation of only 2 wt% of f-RGO. HPU/f-RGO nanocomposite exhibited better electrical conductivity than HPU/RGO nanocomposite at the same nanomaterial content. The formation of a conductive network in the nanocomposite is mainly influenced the electrical conductivity.[60] The large numbers of covalent and noncovalent interactions between f-RGO and HPU chains are present due to uniform distribution of f-RGO sheets in the polymer matrix. Hence, an f-RGO network is formed which helps to create conductive pathways in the nanocomposite. As a result the electrical conductivity is enhanced in HPU/f-RGO nanocomposites from the pristine HPU and HPU/RGO nanocomposite.

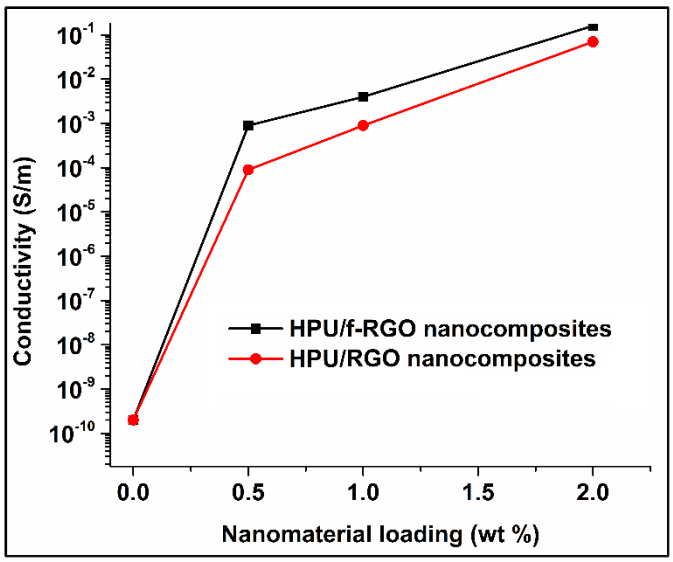

Figure 3C.9 Electrical conductivity of HPU/RGO and HPU/f-RGO nanocomposites

3C.3.7. Shape memory behavior of HPU/RGO and HPU/f-RGO nanocomposites

The multi-stimuli responsive shape memory behavior of the HPU/RGO and HPU/f-RGO nanocomposites was evaluated under sunlight, microwave and thermal heating. Shape memory behavior of HPU/RGO nanocomposite by MW are shown in **Figure 3C.10**. The nanocomposite exhibited excellent shape recovery under the mentioned stimuli. Shape recovery values of the nanocomposite films were faster and more efficient upon exposure to MW and sunlight compared to the thermal stimulus. This may be due to excellent MW and sunlight absorbing capacity of RGO.[52,53] Shape recovery time and ratio under different stimuli are summarized in **Table 3C.3**.

Table 3C.3 Shape memory properties of HPU, HPU/RGO and HPU/f-RGO nanocomposites

Sample	Shape recovery time (min)			Shape recovery ratio (%)		
	MW	Sunlight	Thermal	MW	Sunlight	Thermal
HPU	1.53±0.06	7.1±0.2	6.5±0.1	89.2±0.4	90.1±0.4	88.8±0.4
HPU/f-RGO0.5	1.2±0.09	2.7±0.12	5.6 ±0.16	95.2±0.3	96.4±0.2	95.2±0.3
HPU/f-RGO1	0.9±0.03	1.8±0.06	4.3±0.12	96.6±0.2	97.6±0.2	96.8±0.2
HPU/f-RGO2	0.7±0.06	1.3±0.03	3.1±0.09	98.3±0.2	98.9±0.1	97.6±0.3
HPU/RGO0.5	1.4±0.03	2.7±0.06	5.6±0.15	94.7±0.3	95.9±0.2	94.6±0.2
HPU/RGO1	1.1±0.03	1.8±0.03	4.3±0.12	95.9±0.2	97.1±0.2	96.3±0.2
HPU/RGO2	0.9±0.03	1.3±0.03	3.1±0.09	97.3±0.2	98.2±0.1	97.4±0.3

The shape recovery time decreased with the increase of RGO or f-RGO content in the nanocomposites. Nanomaterial creates a large amount of stored elastic strain energy owing to the presence of strong interfacial interactions with the HPU matrix as mentioned in section 3B.3.4.[42] This helps the nanocomposites to attain a high recovery speed due to the release of stored elastic strain. Energy absorbing capacity from different stimuli also enhances with an increase of the amount of RGO or f-RGO which is another important factor for the fast recovery.

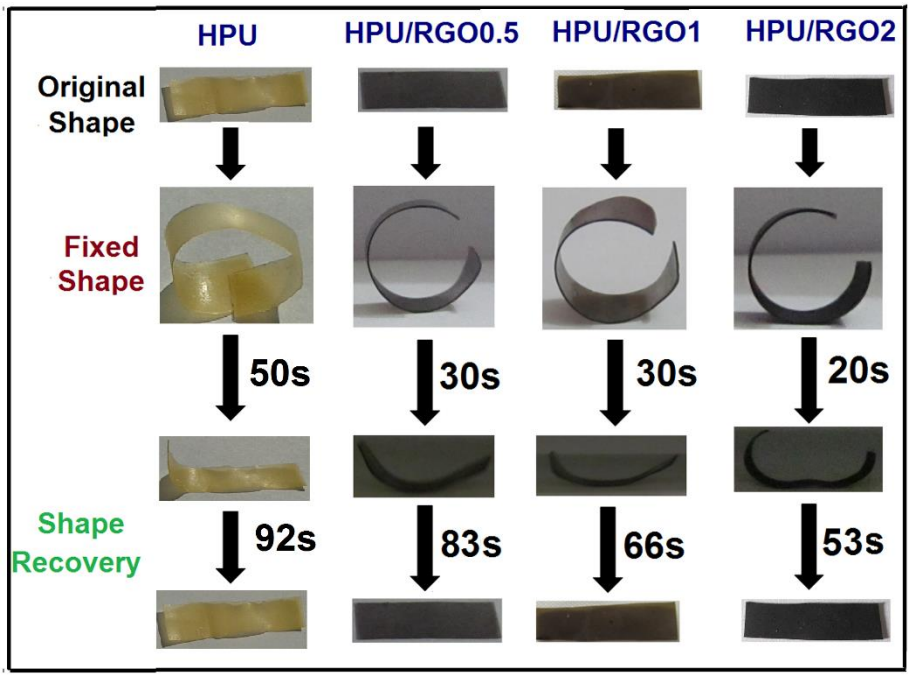

Figure 3C.10 Shape memory behavior of the HPU and HPU/RGO nanocomposite under MW stimulus

3C.4. Conclusion

So, in this study, RGO or f-RGO was used as a reactive chain extender as well as a nano reinforcing material for the fabrication of HPU nanocomposite. HPU/f-RGO nanocomposite exhibited excellent mechanical properties compared to HPU/RGO nanocomposite at the same nanomaterial content. Also, the obtained HPU/f-RGO nanocomposite exhibited excellent electrical conductivity and good multi-stimuli responsive shape memory behavior than HPU/RGO nanocomposite. This study opens the door towards RGO-based nanocomposite as a superior tough conductive smart elastomeric material, which possess a great potential to be used in the fields of aerospace, artificial muscles, tissue engineering, etc.

References

1. Allen, M.J., et al. Honeycomb carbon: a review of graphene, *Chem. Rev.* **110** (1), 132--145, 2010.
2. Lee, C., et al. Measurement of the elastic properties and intrinsic strength of monolayer graphene, *Science* **321**, 385--388, 2008.
3. Balandin, A.A., et al. Superior thermal conductivity of single-layer graphene, *Nano Lett*. **8**, 902--907, 2008.
4. Morozov, S.V., et al. Giant intrinsic carrier mobilities in graphene and its bilayer, *Phys. Rev. Lett.* **100**, 016602 (4 pp), 2008.
5. Bonaccorso, F., et al. Graphene photonics and optoelectronics, *Nat. Photonics* **4**, 611--622, 2010.
6. Hernandez, Y., et al. High-yield production of graphene by liquid-phase exfoliation of graphite, *Nat. Nanotechnol.* **3**, 563--568, 2008.
7. Kim, K.S., et al. Large-scale pattern growth of graphene films for stretchable transparent electrodes, *Nature* **457**, 706--710, 2009.
8. Sutter, P.W., et al. Epitaxial graphene on ruthenium, *Nat. Mater.* **7**, 406--411, 2008.
9. Park, S., & Ruoff, R.S. Chemical methods for the production of graphenes, *Nat. Nanotechnol.* **4**, 217--224, 2009.
10. Shan, C., et al. Water-soluble graphene covalently functionalized by biocompatible poly-L-lysine, *Langmuir* **25** (20), 12030--12033, 2009.
11. Kuila, T., et al. Preparation of functionalized graphene/linear low density polyethylene composites by a solution mixing method, *Carbon* **49** (3), 1033--1037, 2011.
12. Amarnath, C.A., et al. Efficient synthesis of graphene sheets using pyrrole as a reducing agent, *Carbon* **49** (11), 3497--3502, 2011.
13. Huang, X., et al. Graphene-based composites, *Chem. Soc. Rev.* **41**, 666--686, 2012.
14. Mittal, A.K., et al. Synthesis of metallic nanoparticles using plant extracts, *Biotechnol. Adv.* 31 (2), 346--356, 2013.
15. Konwarh, R., et al. Effect of sonication and aging on the templating attribute of starch for "green" silver nanoparticles and their interactions at bio-interface, *Carbohydr. Polym.* **83**, 1245--1252, 2011.
16. Wang, Y., et al. Facile synthesis of soluble graphene via a green reduction of graphene oxide in tea solution and its biocomposites, *ACS Appl. Mater. Interfaces* **3**, 1127--1133, 2011.

17. Akhavan, O., et al. Increasing the antioxidant activity of green tea polyphenols in the presence of iron for the reduction of graphene oxide, *Carbon* **50**, 3015--3025, 2012.
18. Stankovich, S., et al. Stable aqueous dispersions of graphitic nanoplatelets via the reduction of exfoliated graphite oxide in the presence of poly(sodium 4-styrenesulfonate), *J. Mater. Chem.* **16**, 155--158, 2006.
19. Kuila, T., et al. A green approach for the reduction of graphene oxide by wild carrot root, *Carbon* **50** (3), 914--921, 2010.
20. Paredes, J.I., et al. Graphene oxide dispersions in organic solvents, *Langmuir* **24** (19), 10560--10564, 2008.
21. Mei, X., et al. Ultrafast reduction of graphene oxide with Zn powder in neutral and alkaline solutions at room temperature promoted by the formation of metal complexes, *J. Mater. Chem.* **22**, 9109--9116, 2012.
22. Wang, X.X., et al. Carbon nanocages: a new support material for Pt catalyst with remarkably high durability, *Sci. Rep.* **4**, 4437 (pp 11), 2014.
23. Ferrari, A.C., & Basko, D.M. Raman spectroscopy as a versatile tool for studying the properties of graphene, *Nat. Nanotechnol.* **8**, 235--246, 2013.
24. Cui, P., et al. One-pot reduction of graphene oxide at subzero temperatures, *Chem. Commun.* **47**, 12370--12372, 2011.
25. Dey, R.S., et al. A rapid room temperature chemical route for the synthesis of graphene: Metal mediated reduction of graphene oxide, *Chem. Commun.* **48**, 1787--1789, 2012.
26. Akhavan, O., et al. Photodegradation of graphene oxide sheets by TiO_2 nanoparticles after a photocatalytic reduction, *J. Phys. Chem. C* **114** (30), 12955--12959, 2010.
27. Pesika, N.S., et al. Determination of the particle size distribution of quantum nanocrystals from absorbance spectra, *Adv. Mater.* **15**, 1289--1291, 2003.
28. Loh, K.P., et al. Graphene oxide as a chemically tunable platform for optical applications, *Nat. Chem.* **2**, 1015--1024, 2010.
29. Fernandez-Merino, M.J., et al. Vitamin C is an ideal substitute for hydrazine in the reduction of graphene oxide suspensions, *J. Phys. Chem. C* **114** (14), 6426--6432, 2010.
30. Krishnamoorthy, K., et al. Graphene nanosheets: Ultrasound assisted synthesis and characterization, *Ultrason. Sonochem*. **20**, 644--649, 2013.
31. Kuilla, T., et al. Recent advances in graphene based polymer composites, *Prog. Polym. Sci.* **35** (11), 1350--1375, 2010.

32. Rahmat, M., & Hubert, P. Carbon nanotube–polymer interactions in nanocomposites: a review, *Compos. Sci. Technol.* **72**, 72--84, 2011.
33. Moniruzzaman, M., & Winey, K.I. Polymer nanocomposites containing carbon nanotubes, *Macromolecules* **39** (16), 5194--5205, 2006.
34. Zhu, C., et al. Graphene oxide/polypyrrole nanocomposites: One-step electrochemical doping, coating and synergistic effect for energy storage, *J. Mater. Chem.* **22**, 6300--6306, 2012.
35. Wang, X.W., et al. Enhanced performance of biodegradable poly(butylene succinate)/graphene oxide nanocomposites via *in situ* polymerization, *Langmuir* **28**, 7091--7095, 2012.
36. Tiwari, A. & Syväjärvi, M. *Graphene Materials: Fundamentals and Emerging Applications*, John Wiley & Sons, Beverly, 2015.
37. Jing, X., et al. Preparation of thermoplastic polyurethane/graphene oxide composite scaffolds by thermally induced phase separation, *Polym. Compos.* **35**, 1408--1417, 2013.
38. Ponnamma, D., et al. Interrelated shape memory and Payne effect in polyurethane/ graphene oxide nanocomposites, *RSC Adv.* **3**, 16068--16079, 2013.
39. Meng, H., & Li, G. A review of stimuli-responsive shape memory polymer composites, *Polymer* **54**, 2199--2221, 2013.
40. Kalita, H., & Karak, N. Hyperbranched polyurethane/triethanolamine functionalized multi-walled carbon nanotube nanocomposites as remote induced smart materials, *Polym. Int.* **63**, 1295--1302, 2014.
41. Schmidt, A.M. Electromagnetic activation of shape memory polymer networks containing magnetic nanoparticles, *Macromol. Rapid Commun.* **27**, 1168--1172, 2006.
42. Deka, H., et al. Biocompatible hyperbranched polyurethane/multi-walled carbon nanotube composites as shape memory materials, *Carbon* **48**, 2013--2022, 2010.
43. Chen, Z., & Lu, H. Constructing sacrificial bonds and hidden lengths for ductile graphene/ polyurethane elastomers with improved strength and toughness, *J. Mater. Chem.* **22**, 12479--12490, 2012.
44. Gomez-Navarro, C., et al. Elastic properties of chemically derived single graphene sheets, *Nano Lett.* **8**, 2045--2049, 2008.
45. Das, B., et al. Bio-based hyperbranched polyurethane/Fe_3O_4 nanocomposites: Smart antibacterial biomaterials for biomedical devices and implants, *Biomed. Mater.* **8**, 035003 (pp 12), 2013.

46. Karak, N., et al. Synthesis and characterization of castor-oil-modified hyperbranched polyurethanes, *J. Appl. Polym. Sci.* **112**, 736—743, 2009.
47. Liang, J., et al. Molecular-level dispersion of graphene into poly(vinyl alcohol) and effective reinforcement of their nanocomposites, *Adv. Funct. Mater.* **19**, 2297--2302, 2009.
48. Xue, L., et al. Synthesis and characterization of three-arm poly(ε-caprolactone)-based poly(ester−urethanes) with shape-memory effect at body temperature, *Macromolecules* **42**, 964--972, 2009.
49. Sivakumar, C., & Nasar, A.S. Poly(ε-caprolactone)-based hyperbranched polyurethanes prepared via A_2 + B_3 approach and its shape-memory behavior, *Eur. Polym. J.* **45**, 2329--2337, 2009.
50. Lendlein, A., et al. Light-induced shape-memory polymers, *Nature* **434**, 879--882, 2005.
51. Kumpfer, J.R., & Rowan, S.J. Thermo-, photo-, and chemo-responsive shape-memory properties from photo-cross-linked metallo-supramolecular polymers, *J. Am. Chem. Soc.* **133** (32), 12866--12874, 2011.
52. Bai, X., et al. Green approach to prepare graphene-based composites with high microwave absorption capacity, *J. Phys. Chem. C* **115** (23), 11673--11677, 2011.
53. Bernardi, M., et al. Extraordinary sunlight absorption and one nanometer thick photovoltaics using two-dimensional monolayer materials, *Nano Lett.* **13**, 3664--3670, 2013.
54. Tien, H.W., et al. Graphene nanosheets deposited on polyurethane films by self-assembly for preparing transparent, conductive films, *J. Mater. Chem.* **21**, 14876--14883, 2011.
55. Jung, Y.C., et al. Fabrication of transparent, tough, and conductive shape-memory polyurethane films by incorporating a small amount of high-quality graphene, *Macromol. Rapid Commun.* **23**, 628--634, 2012.
56. Park, J., & Yan, M. Covalent functionalization of graphene with reactive intermediates, *Acc. Chem. Res.* **46**, 181--189, 2013.
57. Pei, A., et al. Strong nanocomposite reinforcement effects in polyurethane elastomer with low volume fraction of cellulose nanocrystals, *Macromolecules* **44**, 4422--4427, 2011.

58. Wu, C., et al. Hyperbranched-polymer functionalization of graphene sheets for enhanced mechanical and dielectric properties of polyurethane composites, *J. Mater. Chem.* **22**, 7010--7019, 2012.
59. Khan, U., et al. Development of stiff, strong, yet tough composites by the addition of solvent exfoliated graphene to polyurethane, *Carbon* **48**, 4035--4041, 2010.
60. Raghu, A.V., et al. Preparation and physical properties of waterborne polyurethane/ functionalized graphene sheet nanocomposites, *Macromol. Chem. Phys.* **209**, 2487--2493, 2008.